Article

Depletion with Cyclodextrin Reveals Two Populations of Cholesterol in Model Lipid Membranes

Jonathan P. Litz,[1] Niket Thakkar,[1,2] Thomas Portet,[1] and Sarah L. Keller[1,3,*]
[1]Department of Chemistry, [2]Department of Applied Mathematics, and [3]Department of Physics, University of Washington, Seattle, Washington

ABSTRACT Recent results provide evidence that cholesterol is highly accessible for removal from both cell and model membranes above a threshold concentration that varies with membrane composition. Here we measured the rate at which methyl-β-cyclodextrin depletes cholesterol from a supported lipid bilayer as a function of cholesterol mole fraction. We formed supported bilayers from two-component mixtures of cholesterol and a PC (phosphatidylcholine) lipid, and we directly visualized the rate of decrease in area of the bilayers with fluorescence microscopy. Our technique yields the accessibility of cholesterol over a wide range of concentrations (30–66 mol %) for many individual bilayers, enabling fast acquisition of replicate data. We found that the bilayers contain two populations of cholesterol, one with low surface accessibility and the other with high accessibility. A larger fraction of the total membrane cholesterol appears in the more accessible population when the acyl chains of the PC-lipid tails are more unsaturated. Our findings are most consistent with the predictions of the condensed-complex and cholesterol bilayer domain models of cholesterol-phospholipid interactions in lipid membranes.

INTRODUCTION

Mammalian cells regulate the concentration of cholesterol in their plasma membrane (~40 mol %) and endoplasmic reticulum (~5 mol %). When the concentration of cholesterol in the cell plasma membrane falls below a physiological set point, activation of a signaling pathway results in proteins in the endoplasmic reticulum upregulating cellular cholesterol production (1–3). The cell may maintain this set point by monitoring the chemical activity (effective concentration) of cholesterol in the plasma membrane, which can be significantly different than the total plasma membrane cholesterol concentration (1,4–6). In humans, diets high in saturated fats correlate with hypercholesterolemia, whereas diets high in monounsaturated fats are comparatively hypocholesterolemic (7). The link between saturated fats and hypercholesterolemia may lie in the disparity between the activity and total concentration of cholesterol in the plasma membrane. Cholesterol interacts more favorably with saturated phospholipids than unsaturated phospholipids in membranes (8). These favorable interactions may reduce the activity of cholesterol with respect to total concentration, such that cells with higher concentrations of saturated lipids trigger cholesterol production even when the plasma membrane contains elevated levels of cholesterol.

Direct measurement of the activity of cholesterol in a membrane is difficult. Determining the surface accessibility of cholesterol is more experimentally tractable, and this quantity is hypothesized to be proportional to the activity of cholesterol within the membrane (9). Here, we investigated whether all cholesterol molecules in a two-component PC (phosphatidylcholine) lipid bilayer at high concentrations of cholesterol (30–66 mol %) are equally accessible for removal by methyl-β-cyclodextrin (mβCD). Specifically, we used fluorescence microscopy to image the decrease in area of PC-lipid membranes as mβCD selectively pulled cholesterol from them. We used the rate of decrease in membrane area to determine the rate of cholesterol depletion as a function of both the mole fraction of cholesterol (χ_C) and the degree of unsaturation of the PC-lipid tails. Molecular structures of the three phospholipids studied (DMPC, SOPC, and DOPC in order of increasing acyl-chain unsaturation) and cholesterol are shown in Fig. 1.

Previously, cholesterol-dependent cytolysins and cholesterol oxidase have been used to assay the accessibility of cholesterol in two-component PC-lipid membranes (10–18). The binding of two cytolysins, perfringolysin O and anthrolysin O, to cholesterol in the membrane increases sharply above a single χ_C characteristic to the PC-lipid in the bilayer (10–15). Generally, this χ_C decreases with increasing lipid tail unsaturation. However, slight structural modification of the protein (19) or changes in pH (10) can cause this characteristic χ_C to shift independently of membrane lipid composition. These sensitivities make it difficult to isolate changes in the accessibility of cholesterol from changes in the binding behavior of the cytolysin. The use of monomeric cytolysin subunits likely alleviates this problem (15). Cholesterol oxidase converts cholesterol into cholest-4-en-3-one, altering the composition of the bilayer. This

Submitted September 29, 2015, and accepted for publication November 10, 2015.

*Correspondence: slkeller@chem.washington.edu

Editor: David Cafiso.

0006-3495/16/02/0635/11

http://dx.doi.org/10.1016/j.bpj.2015.11.021

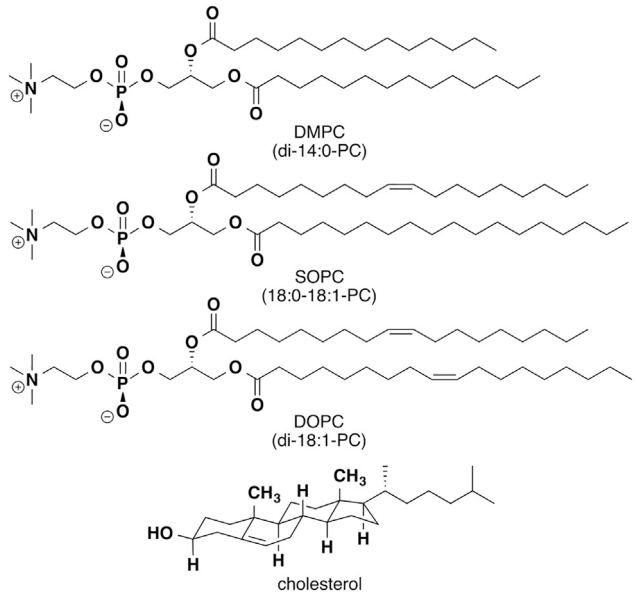

FIGURE 1 The molecular structures of DMPC (di-14:0-PC), SOPC (18:0-18:1-PC), DOPC (di-18:0-PC), and cholesterol. DMPC has two saturated tails. SOPC has one saturated and one monounsaturated tail. DOPC has two monounsaturated tails.

structural change should have minimal impact on the initial rate of oxidation measured, but the eventual widespread replacement of cholesterol, even by structurally similar sterols, can drastically change membrane properties (20,21). There have been disagreements in the literature stemming from the interpretation of results from cholesterol oxidase assays. In particular, some studies claim there is only one χ_C above which cholesterol accessibility increases sharply (16), whereas others claim to observe several spikes in cholesterol oxidase activity at specific values of χ_C (17,18). Results from previous cytolysin and cholesterol oxidase studies on two-component lipid bilayers are summarized in Table 1. Our mβCD area depletion assay avoids significant chemical modification of membrane components while giving an unambiguous readout of the accessibility of cholesterol as a function of χ_C.

There are three significant experimental challenges to overcome in measuring mβCD-induced area depletion of bilayers to determine the accessibility of membrane cholesterol over a wide range of χ_C. First, membrane fluctuations must be suppressed so the decrease in area can be measured accurately. Second, membrane tension must be approximately constant throughout the depletion process so that changes in tension do not influence the measured accessibility; changes in membrane tension makes measurements involving vesicles problematic (22,23). Third, knowledge is needed of the area per molecule of the membrane as a function of cholesterol concentration. This quantity is straightforward to measure for monolayers (24) but much more challenging to determine for bilayers (25). We addressed the first two challenges by developing

TABLE 1 Previously Published Measurements of Cholesterol Accessibility for Two-Component PC-Lipid Bilayers

PC-Lipid[a]	Characteristic χ_C[b]	Assay	Reference
di-16:0	0.63, 0.58	COD	(18)
	0.50	COD	(16)
di-14:0	0.50	COD	(16)
18:0-18:1	0.50	COD	(16)
16:0-18:1	0.58, 0.52, 0.40, 0.25	COD	(18)
	0.50	COD	(16)
	0.334, 0.250	COD	(17)[c]
di-18:1	0.62, 0.57, 0.51, 0.40, 0.25	COD	(18)
	0.33	COD	(16)
di-18:0	0.47[d]	PFO	(11)
di-16:0	0.49[d]	PFO	(11)
di-14:0	0.51[d]	PFO	(11)
18:0-18:1	0.42[d]	PFO	(11)
16:0-18:1	0.47[d]	PFO	(14)
	0.45[d]	PFO	(14)
	0.45	PFO	(12)
	0.44[d]	PFO	(11)
	0.44[d]	PFO	(13)
	0.28[d]	PFO, pH = 7.4	(10)
	0.24[d]	PFO, pH = 5.1	(10)
di-18:1	0.45	PFO-D4[e]	(15)
	0.45	ALO-D4[e]	(15)
	0.41	PFO	(15)
	0.37[d]	PFO	(11)
	0.35	PFO	(12)
	0.34[d]	PFO	(14)
	0.26	ALO	(15)
	0.26[d]	PFO, pH = 7.4	(10)
	0.20[d]	PFO, pH = 7.0	(10)
di-(4Me-16:0)	0.31	PFO	(15)
	0.27	PFO-D4[e]	(15)
	0.27	ALO-D4[e]	(15)
	0.25	PFO	(12)

COD, cholesterol oxidase; PFO, perfringolysin O; ALO, anthrolysin O.
[a]Lipids are listed by the number of carbons and degree of unsaturation of their tails (e.g., DMPC is di-14:0-PC).
[b]Characteristic χ_C refers to the one or several mole fraction(s) of cholesterol at or above which the accessibility of cholesterol increases sharply. Only characteristic $\chi_C \geq 0.20$ are listed.
[c]The researchers did not report on bilayers with $\chi_C > 0.345$.
[d]This value was interpreted from a graph as the half-maximum of cytolysin binding.
[e]This version of the protein is monomeric and does not cause pores to form in the membrane.

a method of rupturing biotinylated giant unilamellar vesicles (GUVs) onto a glass substrate coated with streptavidin that yields supported lipid bilayers (SLBs). Upon depletion of cholesterol with mβCD, a few large holes form in the bilayer, suggesting that strong bilayer-surface pinning interactions are minimized. We tackled the third challenge by aggregating published bilayer thickness and area per unit cell data and converting those values to molecular areas. An overview of our experimental procedure is shown in Fig. 2 (full details appear in the Materials and Methods).

It is important that we conduct our experiments on bilayers rather than monolayers—as has been achieved

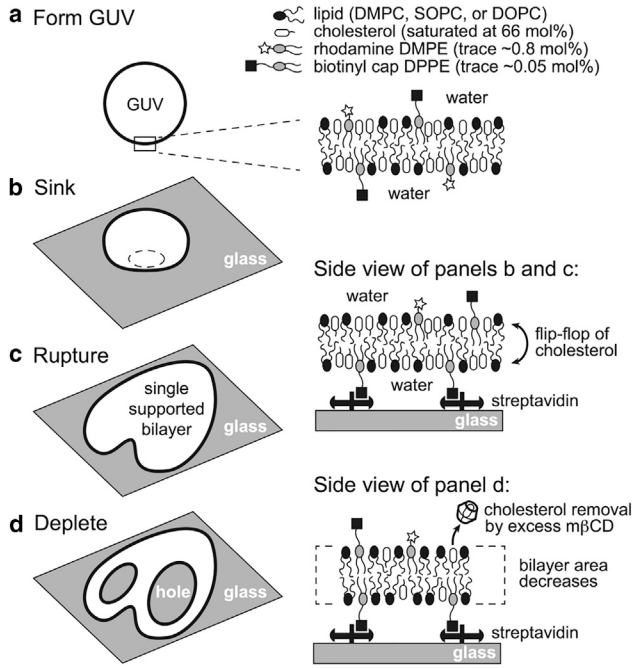

FIGURE 2 Overview of the experimental procedure. (*a*) A GUV saturated with cholesterol at 66 mol % is produced via electroformation. (*b*) The GUV sinks to the bottom of the experimental chamber. (*c*) It then ruptures onto a streptavidin-functionalized glass coverslip, forming a heart-shaped SLB. Cholesterol flip-flop is rapid between the upper and lower leaflets of the fluid bilayer (39–42). (*d*) mβCD is added to the chamber, where it selectively removes cholesterol from the SLB. Large holes form in the SLB as cholesterol is depleted, and the bilayer area decreases.

previously (9)—because large differences in miscibility behavior between monolayer and bilayer systems imply that cholesterol-phospholipid interactions differ in the two systems (26). Also, our goal is to resolve disagreements about which models of cholesterol-lipid interactions best describe the accessibility of cholesterol in bilayer systems. The clearest predictions from these models apply to bilayers comprised of a single lipid and cholesterol, which led us to use binary membranes in our experiments. Membranes composed of certain ternary mixtures of lipids and cholesterol are known to phase-separate at common experimental temperatures (27). Reports of two rates of cholesterol efflux from cells and from bilayers composed of ternary lipid mixtures (22,28–30) are challenging to interpret if the membrane demixes into coexisting liquid phases.

Here we show that the accessibility of cholesterol for removal by mβCD increases sharply above a single characteristic χ_C specific to the PC-lipid in the membrane. Our membranes are free of macroscopic phase separation. Our results show that cholesterol exists in multiple populations with distinct accessibilities in two-component PC-lipid membranes that appear otherwise homogeneous. Our method enables us to distinguish between different models of cholesterol-phospholipid interactions in lipid bilayers.

MATERIALS AND METHODS

Chemicals

DMPC (1,2-dimyristoyl-*sn*-glycero-3-phosphocholine, di-14:0-PC), SOPC (1-stearoyl-2-oleoyl-*sn*-glycero-3-phosphocholine, 18:1-18:0-PC), DOPC (1,2-dioleoyl-*sn*-glycero-3-phosphocholine, di-18:1-PC), biotinyl cap DPPE (1,2-dipalmitoyl-*sn*-glycero-3-phosphoethanolamine-*n*-(cap biotinyl), and rhodamine DMPE (1,2-dimyristoyl-*sn*-glycero-3-phosphoethanolamine-*n*-(lissamine rhodamine B sulfonyl) were from Avanti Polar Lipids (Alabaster, AL). Cholesterol was from Sigma-Aldrich (St. Louis, MO). All lipids were used without further purification and were stored at −20°C. Biotinyl cap DPPE was stored in chloroform/methanol/water (65:35:8 by volume), and all other lipids were stored in chloroform. Streptavidin and mβCD were from Sigma-Aldrich. Glucose and sucrose were from Fisher Scientific (Waltham, MA). All water was purified to 18 MΩ-cm with a Barnstead filtration system from Thermo Scientific (Waltham, MA).

Giant unilamellar vesicle formation

GUVs were generated by electroformation as in previous experiments (Fig. 2 *a*) (27). Electroformation was conducted using mixtures of PC-lipid/cholesterol/rhodamine DMPE/biotinyl cap DPPE (25:75:0.8:0.05 by mole) to produce GUVs saturated in cholesterol at 66 mol %; excess cholesterol precipitates as crystalline cholesterol monohydrate (21,31). Briefly, 0.25 mg of lipids were dissolved in chloroform and spread onto two 37.5 × 25 mm glass slides coated with indium-tin-oxide (Delta Technologies, Loveland, CO). The lipid-coated slides were placed under vacuum for 30 min to remove solvent. Pairs of slides were assembled face-to-face separated by a 1-mm gap maintained by two Teflon spacers. The gap was filled with 200 mM sucrose, and the edges were sealed with vacuum grease. The two indium-tin-oxide surfaces were connected to an AC voltage of 1.5 V at 10 Hz for 1 h at 60°C. The resulting GUV-rich solution was diluted with 3.5 mL of 200 mM sucrose at 60°C, then cooled to room temperature (24–26°C). This temperature is above the gel-liquid coexistence temperature of all vesicles studied (32,33). All experiments reported here featured vesicles that ruptured smoothly onto solid supports and that exhibited uniform distributions of dye-labeled lipids. We find that vesicles in the gel phase (e.g., 100% DMPC vesicles below 24°C) often do not rupture smoothly and that the dye-labeled lipids often accumulate at the edges of the resulting SLBs. Experiments were performed within 4 h of vesicle formation.

Supported lipid bilayer formation and cholesterol depletion

A 25 × 25 mm glass coverslip (Fisher Scientific) was plasma-etched (Harrick, Ithaca, NY) for 50 s. A quantity of 1.5 mL of 0.1 mg/mL streptavidin in water was deposited on the coverslip. After 20 min, the water was poured off, and the coverslip was adhered with vacuum grease to form the base of a cylindrical well with a radius of 10 mm and a height of 12 mm. The chamber was gently rinsed with water five times and placed on the stage of an inverted epifluorescence microscope.

One milliliter of 200 mM glucose was added to the chamber, followed by 20–50 μL of GUV-rich solution. GUVs sank to the bottom of the chamber (Fig. 2 *b*). Within 1–2 min, hundreds of vesicles ruptured onto the coverslip to create a field of heart-shaped SLBs spatially separated by bare glass (Figs. 2 *c* and 3). The asymmetric rupture mechanism that produces heart-shaped SLBs has been explored previously (34), and we found our protocol predominantly yields this rupturing pattern. The chamber was washed with 1 mL of 200 mM glucose 10 times. Care was taken to ensure that SLBs were never directly exposed to air. After an initial image was collected, 2 mL of 3.75 mM (for membranes with DMPC or SOPC) or 1.5 mM (for membranes with DOPC) mβCD in 200 mM aqueous glucose was added to the experimental chamber, yielding 3 mL of 2.5 mM (for

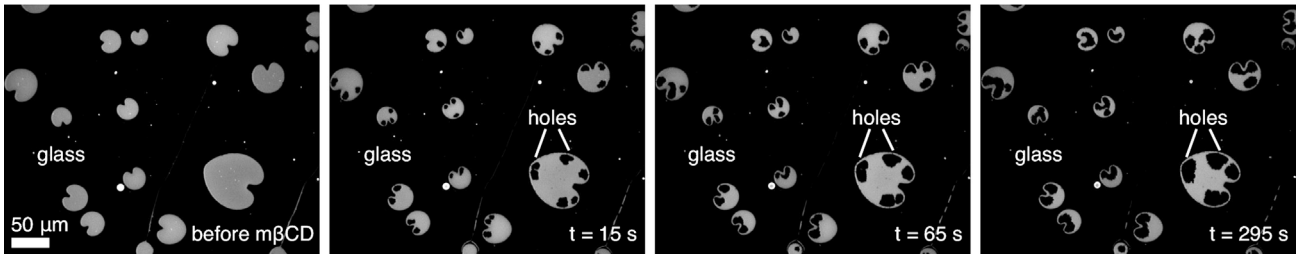

FIGURE 3 Micrographs of the cholesterol depletion process. Heart-shaped regions (*gray*) are individual supported lipid bilayers formed from the rupture of giant unilamellar vesicles onto a glass coverslip (*black*). mβCD is added at $t = 0$ s. mβCD removes cholesterol from the supported lipid bilayers. Large holes form in the bilayers as their areas decrease, further revealing the glass coverslip beneath them. DMPC/cholesterol bilayers are shown here, [mβCD] = 2.5 mM.

membranes with DMPC or SOPC) or 1 mM (for membranes with DOPC) mβCD in 200 mM aqueous glucose. Approximately 5 s later, images were collected every 2 s with 500 ms exposures for a total of 300 s (DMPC or DOPC) or 100 s (SOPC) (Figs. 2 *d* and 3). All experiments were performed at 24–26°C. Two different concentrations of mβCD were used because 2.5 mM mβCD removes cholesterol from DOPC bilayers too quickly to accurately measure the rate of area depletion, whereas 1 mM mβCD depletes cholesterol prohibitively slowly from SOPC and DMPC bilayers. In total, we obtained data from 82 distinct bilayers of cholesterol with DMPC, 95 with SOPC, and 49 with DOPC.

At concentrations <5–20 mM, mβCD selectively removes cholesterol from PC-lipid bilayers, leaving the phospholipids behind and the membrane intact (35–38). As a control to ensure that our procedure does not remove significant amounts of PC-lipids from the bilayer, we performed our assay using SLBs of pure DMPC, SOPC, or DOPC. No area depletion was observed on the timescale of our experiment.

It is likely that mβCD pulls cholesterol from only the upper leaflet of the SLBs. Because the rate of cholesterol flip-flop is on the order of milliseconds in fluid phase lipid bilayers (39–42) and our experiment occurs on the order of seconds, we expect that cholesterol equilibrates across the leaflet of our bilayers faster than we could detect. If cholesterol flip-flop were hindered and cholesterol could only move between the two leaflets by edge diffusion, we would expect to see depletion rates vary with SLB size. We found no correlation between SLB size and cholesterol depletion rate (see Fig. S1 in the Supporting Material), nor did we find evidence of an asymmetric distribution of cholesterol across the two leaflets in our observations.

Images and image processing

Epifluorescence microscopy was performed with a 10× objective on an inverted microscope (Nikon, Melville, NY) with a Coolsnap *fx* charge-coupled device camera (Photometrics, Tucson, AZ). All micrographs were analyzed using the open-source software package Fiji (43). Each time series of images was converted to a series of binary images using Fiji's isodata algorithm. The number of pixels in each SLB as a function of time was determined using Fiji's Analyze Particles function. The fraction of bilayer area remaining is determined by dividing the area remaining of each bilayer by its initial area. We imaged 3–15 separate SLBs per experiment. Data for any bilayer with an initial area of fewer than 250 μm^2 was discarded to limit sensitivity to noise in the area measurement. Occasionally, over the course of an experiment, a free-floating GUV or other lipid debris drifted over one of the bilayers being imaged, briefly obfuscating measurement of the bilayer area. In this case, the affected data points were discarded.

Curve fitting

We fit all data using the freely available Python module PyMC (44). PyMC implements Markov chain Monte Carlo algorithms to provide a computationally tractable approach to Bayesian curve fitting. For each fit, we started with a uniform prior probability distribution and generated 100,000 samples of the posterior distribution using a likelihood function that assumes independent, unbiased, and normally distributed errors in the data. The first 20,000 of these samples were discarded as burn-in to avoid sampling from the Markov chain before it reached its equilibrium distribution. We determined the means and standard deviations of fitting parameters and derived values in the results directly from these sets of 80,000 samples (see Fig. S2 for plots of the sampled posterior distribution).

Bilayer area per molecule

We aggregated published bilayer electron density peak-to-peak distances, d_{pp}, determined by x-ray diffraction (45–47) and area per unit cell data, A_{UC}, determined by neutron scattering (48,49) or jointly analyzed neutron and x-ray scattering (50,51) for bilayers comprised of cholesterol and either DMPC, SOPC, or DOPC at 30°C (see Tables S1–S5 in the Supporting Material for all data used).

From x-ray experiments, we determined the thickness of the approximately incompressible hydrocarbon region of the bilayer as a function of mole fraction of cholesterol, $d_{HC}(\chi_C)$, as

$$d_{HC}(\chi_C) = d_{pp}(\chi_C) - 2d_{H1}, \tag{1}$$

where d_{H1} is the distance from the peak of the x-ray scattering electron density profile to the interface of the hydrocarbon region of the bilayer, as determined by the joint analysis of x-ray and neutron scattering data for single-component bilayers consisting of the appropriate PC-lipid (50,51). It is likely that d_{H1} varies with χ_C, but there are no published values of this relationship for the systems we studied. We therefore approximated d_{H1} as constant with respect to χ_C.

From d_{HC}, we determined the average area per molecule in the bilayer, a_{avg}, as

$$a_{\text{avg}}(\chi_C) = \frac{2V_{HC}(\chi_C)}{d_{HC}(\chi_C)}, \tag{2}$$

where V_{HC} is the average volume per molecule in the hydrophobic portion of the bilayer, computed as

$$V_{HC}(\chi_C) = (V_L - V_H) \times (1 - \chi_C) + V_C\chi_C, \tag{3}$$

and where V_L, V_H, and V_C are the reported volumes of the PC-lipid (52,53), the PC-headgroup (54,55), and a single cholesterol molecule in a PC-lipid bilayer (53), respectively. It is likely that cholesterol does not lie entirely within the hydrocarbon portion of the bilayer (14,46), but no value for the fraction of excluded volume has been reported. We therefore approximated cholesterol as being completely located within the hydrocarbon region of the bilayer.

From neutron scattering experiments, we determined a_{avg} as

$$a_{avg}(\chi_C) = A_{UC}(\chi_C) \times (1 - \chi_C). \quad (4)$$

We found that a_{avg} is well described as exponentially increasing with decreasing χ_C,

$$a_{avg}(\chi_C) \approx p_1 + p_2 e^{-p_3 \chi_C}, \quad (5)$$

where p_1, p_2, and p_3 are the fitting parameters (see Fig. 4). The fitting parameters are summarized in Table 2. We do not assign a physical meaning to these fitting parameters or relationship, and we use this analytic form only as an approximation of a_{avg} to enable further analysis.

RESULTS

We added mβCD to an aqueous solution above a field of SLBs and recorded a time-series of micrographs to determine the rate at which cholesterol is depleted from the lipid bilayers. Full experimental details are compiled in the Materials and Methods. A representative time-series of images for bilayers of DMPC and cholesterol appears in Fig. 3. We collected similar time-series for bilayers of SOPC and cholesterol and for bilayers of DOPC and cholesterol. As cholesterol is depleted from each bilayer, a few holes form and grow. We plot the fraction of each bilayer area remaining as a function of time after mβCD is added, $A_R(t)$. In Fig. 5 the mean of the experimental data $\pm$ two standard errors is shown in black, and the standard deviation of the data is shown in gray. Our goal is to use $A_R(t)$ to quantitatively determine how the rate of cholesterol depletion depends on χ_C.

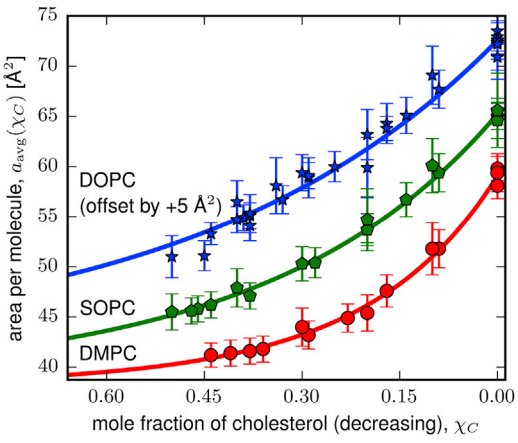

FIGURE 4 The average area per molecule as a function of mole fraction of cholesterol, a_{avg} (χ_C), for two-component bilayers of cholesterol with DMPC (*circles*, *red line*), SOPC (*pentagons*, *green line*), or DOPC (*stars*, *blue line*). All data (*symbols*) shown here are determined from previously reported measurements of bilayer thickness or area per unit cell conducted at 30°C (45–51). The average area per molecule is well approximated as exponentially increasing with decreasing cholesterol mole fraction (*colored lines*). DOPC data is offset (increased) by 5 Å^2 to avoid overlap with the SOPC data. To see this figure in color, go online.

TABLE 2 Fitting Parameters for the Average Area per Molecule in a Bilayer as a Function of Mole Fraction of Cholesterol, $a_{avg}(\chi_C)$

Lipid	p_1 (Å^2)	p_2 (Å^2)	p_3
DMPC	38.1 ± 2.4	21.0 ± 2.4	5.1 ± 1.4
SOPC	38.5 ± 3.0	26.8 ± 2.9	2.9 ± 0.7
DOPC	36.5 ± 2.1	31.1 ± 2.1	2.2 ± 0.3

The method of generating uncertainties in the fitting parameters is described in the Curve Fitting subsection.

Our approach to analyzing $A_R(t)$ is as follows. We define

$$A_R(t) \equiv \frac{\text{area of bilayer at } t}{\text{area of bilayer at } t = 0} = \frac{n_L + n_C(t)}{n_L + n_C(0)} \times \frac{a_{avg}(\chi_C[t])}{a_{avg}(\chi_C[0])}, \quad (6)$$

$$= \left(1 - \chi_C(0) + \frac{n_C(t)}{n_L + n_C(0)}\right) \times \frac{a_{avg}(\chi_C[t])}{a_{avg}(\chi_C[0])}, \quad (7)$$

where n_L is the number of PC-lipid molecules initially in the bilayer, χ_C is the mole fraction of cholesterol in the bilayer, n_C is the monotonically decreasing number of cholesterol molecules in the bilayer, and a_{avg} is the composition-dependent average area per molecule in the bilayer.

Because we deplete with a gross excess of mβCD, the concentration of mβCD remains approximately constant throughout the experiment. Therefore, the rate of depletion for a given SLB varies with n_C only. If all cholesterol in the bilayer were equally accessible by mβCD and this accessibility were independent of χ_C, then the rate law governing the depletion process would be pseudo-first order in n_C with

$$-\frac{dn_C(t)}{dt} = k_1 n_C(t), \quad (8)$$

$$n_C(t) = n_C(0) e^{-k_1 t}, \quad (9)$$

where k_1 is the depletion rate constant. Then by Eq. 7,

$$A_R(t) = \left(1 - \chi_C(0) + \frac{n_C(0)}{n_L + n_C(0)} e^{-k_1 t}\right) \times \frac{a_{avg}(\chi_C[t])}{a_{avg}(\chi_C[0])}, \quad (10)$$

$$= \left(1 - \chi_C(0) + \chi_C(0) e^{-k_1 t}\right) \times \frac{a_{avg}(\chi_C[t])}{a_{avg}(\chi_C[0])}, \quad (11)$$

where k_1 is the single fitting parameter used to generate the one-population fit shown in Fig. 5 (*blue line*). This model underfits our data, implying that a model in which all cholesterol in the membrane is in a single population is inadequate to describe our system.

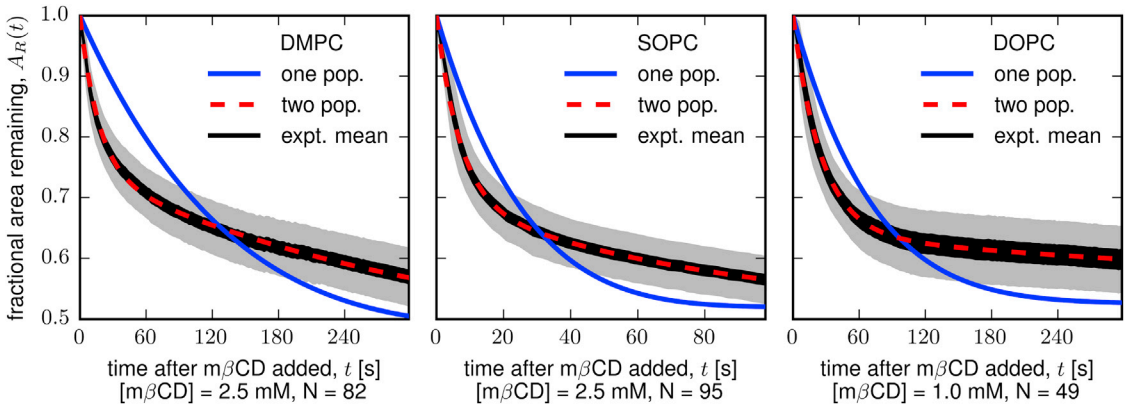

FIGURE 5 The fraction of bilayer area remaining as a function of time, $A_R(t)$, after addition of mβCD. $A_R(t)$ decreases as mβCD depletes cholesterol from the bilayer. (*Black region*) Our experimental mean ± 2 SE; (*gray region*) standard deviation of our data. The model with two cholesterol populations describes the data well (*red dotted line*), whereas the model with only one cholesterol population underfits the data (*blue line*). N is the number of replicate bilayers studied. To see this figure in color, go online.

If instead there were two independent populations of cholesterol, one with high accessibility and one with low accessibility, then the depletion would be the sum of two pseudo-first-order processes with

$$-\frac{dn_C(t)}{dt} = k_s n_s(t) + k_f n_f(t), \tag{12}$$

$$n_C(t) = n_s(0)e^{-k_s t} + n_f(0)e^{-k_f t}, \tag{13}$$

where n_f and n_s are the numbers of cholesterol molecules in the two populations with corresponding rate constants k_f and k_s. We choose $k_f > k_s$ so that k_f (k_s) represents the fast (slow) cholesterol population. By Eq. 7,

$$A_R(t) = \left(1 - \chi_C(0) + \frac{n_s(0)}{n_L + n_C(0)}e^{-k_s t} + \frac{n_f(0)}{n_L + n_C(0)}e^{-k_f t}\right) \times \frac{a_{\text{avg}}(\chi_C[t])}{a_{\text{avg}}(\chi_C[0])}. \tag{14}$$

We then use the fact that $n_f(0) = n_C(0) - n_s(0)$, and define χ_s^0 as the initial mole fraction of the slow population of cholesterol, $\chi_s^0 \equiv n_s(0)/(n_L + n_C(0))$, to obtain

$$A_R(t) = \left(1 - \chi_C(0) + \chi_s^0 e^{-k_s t} + (\chi_C(0) - \chi_s^0)e^{-k_f t}\right) \times \frac{a_{\text{avg}}(\chi_C[t])}{a_{\text{avg}}(\chi_C[0])}, \tag{15}$$

where χ_s^0, k_s, and k_f are the three fitting parameters used to generate the two-population fit shown in Fig. 5 (*red dotted line*). This model describes our data well, and a summary of the fitting parameters is given in Table 3. This model is the simplest description of a membrane with more than one population of cholesterol. It is possible that there are more than two populations of cholesterol or that the two populations readily interconvert, but adding further complexity to the model is unwarranted by our data (see Fig. S3 for a three-population model).

TABLE 3 Experimental Parameters and Fitting Results for the Two-Population Model of Cholesterol

Lipid	N[a]	[mβCD] (mM)[b]	χ_s^0[c]	$k_s \times 10^3$ (s^{-1})[d]	$k_f \times 10^3$ (s^{-1})[e]
DMPC	82	2.5	0.391 ± 0.002	2.38 ± 0.03	57.4 ± 1.2
SOPC	95	2.5	0.312 ± 0.004	8.2 ± 0.2	138.2 ± 3.9
DOPC	49	1.0	0.226 ± 0.004	0.98 ± 0.10	36.7 ± 0.8

The method of generating uncertainties in the fitting parameters is described in the Curve Fitting subsection.
[a]The number of replicate bilayers measured.
[b]The concentration of mβCD used (see the Materials and Methods).
[c]Fitting parameter corresponding to the initial mole fraction of the slow population of cholesterol.
[d]Fitting parameter corresponding to the rate constant for the depletion of the slow population of cholesterol.
[e]Fitting parameter corresponding to the rate constant for the depletion of the fast population of cholesterol.

DISCUSSION

We found evidence for two populations of cholesterol in bilayers containing cholesterol and either DMPC, SOPC, or DOPC. The fraction of cholesterol that is more highly accessible increases with the degree of unsaturation of the PC-lipid's acyl chains. These results, in conjunction with the previous literature results in Table 1, enable us to assess current models of cholesterol-phospholipid interactions.

Models of cholesterol-phospholipid interactions

There are four commonly referenced descriptions of cholesterol-phospholipid interactions in membranes that yield distinct predictions about how the accessibility of

cholesterol should vary with composition. These are the umbrella, superlattice, condensed-complex, and cholesterol bilayer domain models (Table 4).

At the solubility limit of cholesterol in the bilayer, the umbrella model predicts nonspecific cholesterol-phospholipid interactions that are independent of the PC-lipid tail (56). The large hydrophilic PC-headgroups form a protective canopy under which cholesterol diffuses freely. Each PC-umbrella shields up to two molecules of cholesterol from water. This model successfully predicts that the solubility limit of cholesterol in PC-lipid bilayers is largely independent of PC-lipid tail structure (31), with notable exceptions being polyunsaturated (57,58) and methylated (59) PC-lipids. However, by the shielding mechanism alone, all cholesterol in the bilayer should be equally accessible for removal by mβCD. Our results provide evidence that there are at least two populations of cholesterol with distinct accessibilities, and treating all cholesterol as equally accessible underfits our data (Fig. 5, *blue line*).

Both the umbrella and superlattice models predict that bilayers contain latticelike, regular distributions of cholesterol and phospholipids at several characteristic values of χ_C. By the umbrella model, lattice formation is driven by unfavorable multibody cholesterol-phospholipid interactions; the energy of these interactions increases nonlinearly as the number of cholesterol molecules per phospholipid increases (56). By the superlattice model, long-range cholesterol-cholesterol repulsions drive lattice formation (60). An essential similarity between these models is that both claim that the characteristic χ_C at which regular distributions form are independent of the degree of unsaturation of the PC-lipid tail (18,56). The results reported in Wang et al. (17) and Ali et al. (18) are consistent with some of the predictions of these models. However, our results clearly show that the accessibility of cholesterol depends on the PC-lipid tail, with starkly different values of χ_s^0, k_s, and k_f for the three PC-lipids studied (Table 3). These models also predict a change in cholesterol accessibility at several values of χ_C. Our results show that a two-population model of cholesterol with a single characteristic χ_C is sufficient to describe our systems.

TABLE 4 Summary of Models of Cholesterol-Phospholipid Interactions in Lipid Membranes

Model	Number of Characteristic χ_C[a] ($0.66 > \chi_C > 0.30$)	Dependent on PC-Lipid Head or Tail?[b]
Umbrella (at solubility limit)	0	head
Condensed-complex	1	tail
Cholesterol bilayer domain	1	both
Umbrella (regular distributions)	≥ 3	head
Superlattice	≥ 3	head

[a]The number of characteristic χ_C at which the accessibility of cholesterol is predicted to change sharply.
[b]Statement of whether the predictions of the model vary with the structure of the phospholipid head, tail, or both.

The third model, the condensed-complex model, predicts that cholesterol and phospholipids react reversibly to form thermodynamically stable complexes with a well-defined stoichiometry characteristic to the phospholipid tail (61). These complexes behave as a third chemical species in the two-component bilayer. Cholesterol accessibility increases once χ_C exceeds the complex stoichiometry. At this point, the population of cholesterol that is more accessible exists in excess of the amount of cholesterol needed to fully partner with each PC-lipid. Our results, as well as many results reported in the literature (10–16), are consistent with this model. We found our data are well described with two populations of cholesterol and that the characteristic χ_C at which cholesterol accessibility begins to increase varies with the degree of unsaturation of the PC-lipid tail.

The fourth model, the cholesterol bilayer domain model, states that cholesterol in excess of a threshold mole fraction, χ_{CBD}, forms submicroscopic domains of bilayer-thick, tail-to-tail cholesterol monohydrate that are soluble in the membrane (62–65). Signatures of these domains in two-component PC-lipid bilayers have been interpreted from x-ray diffraction, neutron scattering, and electron paramagnetic resonance (Table 5) (45,66–70). Our results are also consistent with this model. The characteristic χ_C at which cholesterol accessibility begins to increase would correspond to the formation of cholesterol bilayer domains made of cholesterol in excess of χ_{CBD}; cholesterol in these domains would be less shielded from the aqueous phase than those in PC-lipid rich regions.

These four models need not be mutually exclusive. The cholesterol bilayer domain model makes predictions only about cholesterol concentrations above χ_{CBD}; it does not preclude the predictions of the condensed-complex model or the regular distributions predicted by the superlattice or umbrella models below χ_{CBD}. Attempts have been made to resolve the condensed-complex and superlattice models by treating the condensed-complexes as subunits that aggregate to form larger superlattice clusters over time (71). Also, for $\chi_C < 0.50$, the umbrella and superlattice models yield similar characteristic values of χ_C (56).

TABLE 5 Experimental Reports of Cholesterol Bilayer Domains in Two-Component PC-Lipid Bilayers

PC-Lipid[a]	χ_{CBD}[b]	Technique	Reference
di-14:0	0.50	electron paramagnetic resonance	(69)
16:0-18:1	0.50		(67)
di-16:0	0.325	neutron scattering	(70)
di-16:0	0.54 ± 0.02	x-ray diffraction	(66)
di-14:0	0.44		(45)
	0.40		(68)
18:0-18:1	0.47		(45)
di-18:1	0.40		(45)

[a]Lipids are listed by the number of carbons and degree of unsaturation of their tails (e.g., DMPC is di-14:0-PC).
[b]The mole fraction of cholesterol above which signatures of cholesterol bilayer domains are reported.

Condensed-complex stoichiometry and χ_{CBD}

From our two-cholesterol population model, we derived values pertinent to the condensed-complex and cholesterol bilayer domain models (Table 6). We determined the values of the phospholipid-cholesterol complex stoichiometries that result from applying the condensed-complex model to our data. This stoichiometry is equivalent to the ratio of the number of cholesterol molecules in the less accessible (slow) pool to the total number of PC-lipid molecules in the bilayer. We compute this ratio as

$$\text{complex stoichiometry} = \frac{n_s(0)}{n_L} = \frac{\chi_s^0}{1-\chi_C(0)}. \quad (16)$$

In the context of the cholesterol bilayer domain model, we determine the mole fraction of cholesterol above which cholesterol bilayer domains would form in the bilayer, χ_{CBD}. This quantity is approximated by assuming that all cholesterol in the more accessible population is located in cholesterol bilayer domains. This value is most directly comparable to the characteristic χ_C values reported in Table 1. We determine

$$\chi_{CBD} = \frac{n_s(0)}{n_L + n_s(0)} = \frac{\chi_s^0}{1-\chi_C(0)+\chi_s^0}. \quad (17)$$

We also compute the ratio of the depletion rate constants of the two populations of cholesterol (k_f/k_s).

Depletion rate coefficient

Because the two-component membranes we investigate appear homogeneous, it is natural to think of the depletion process as pseudo-first order in n_C with a composition-dependent rate coefficient of depletion, k_D:

$$-\frac{dn_C(t)}{dt} = k_D(\chi_C[t])n_C(t), \quad (18)$$

$$k_D(\chi_C[t]) = \frac{-1}{n_C(t)}\frac{dn_C(t)}{dt}, \quad (19)$$

$$= \frac{-1}{\chi_C(t)(1-\chi_C(t))}\frac{d\chi_C(t)}{dt}. \quad (20)$$

Our depletion rate coefficient is proportional to the average accessibility of all cholesterol in the bilayer. Encapsulated within k_D is the effect of the concentration of mβCD on the rate of depletion. For purposes of comparison with other literature values, we treat the depletion as second order in mβCD (35) and therefore scale our results for k_D of DOPC by a factor of 6.25 (2.5^2) to account for differences in the concentration of mβCD used (Table 3).

In Fig. 6, we show that, at a given χ_C, k_D increases with the degree of unsaturation of the PC-lipid tails. This is consistent with cholesterol interacting more favorably with saturated lipids than unsaturated lipids (8). The value of k_D decreases sharply as the more readily accessible population of cholesterol is depleted. The proportion of cholesterol in this population at high χ_C increases with the degree of lipid tail unsaturation.

TABLE 6 Values Derived from a Two-Population Model of Cholesterol

Lipid	Complex Stoichiometry[a]	χ_{CBD}[b]	k_f/k_s[c]
DMPC	1.150 ± 0.006	0.535 ± 0.001	24.1 ± 0.4
SOPC	0.92 ± 0.01	0.479 ± 0.004	16.8 ± 0.4
DOPC	0.67 ± 0.01	0.399 ± 0.005	37.9 ± 3.3

The method of generating uncertainties is described in the Curve Fitting subsection.

[a]The average number of cholesterol molecules complexed with a single PC-lipid molecule in the context of the condensed complex-model.

[b]The mole fraction of cholesterol above which cholesterol bilayer domains would be expected to exist in the context of the cholesterol bilayer domain model. This value is most directly comparable to the characteristic χ_C values in Table 1.

[c]The ratio of depletion rate constants between the fast and slow populations of cholesterol.

Advantages and disadvantages of the mβCD area depletion assay

With our area depletion assay, a single experiment yields data for up to 15 individual SLBs over a wide range of cholesterol concentrations, enabling rapid acquisition of replicate data.

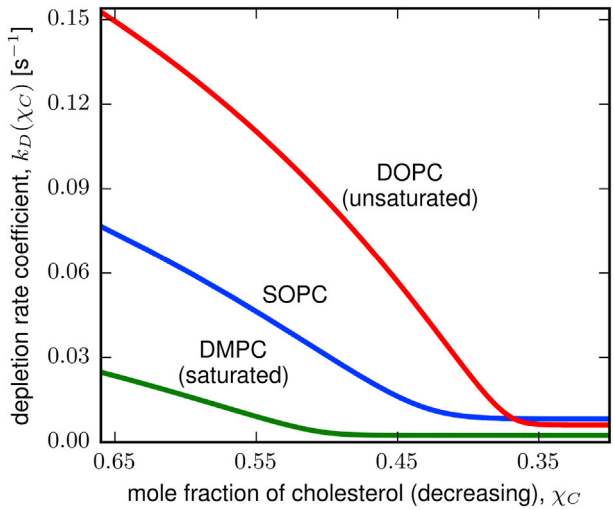

FIGURE 6 The depletion rate coefficient as a function of the mole fraction of cholesterol in the bilayer, $k_D(\chi_C)$. The rate coefficient decreases sharply as the more accessible population of cholesterol is depleted. The fraction of cholesterol in this population increases with increasing PC-lipid tail unsaturation from DMPC (*green*) to SOPC (*blue*) to DOPC (*red*). At a given χ_C, the rate coefficient increases with increasing lipid tail unsaturation. We treat the depletion process as second order in mβCD (35) and scale k_D for DOPC by a factor of 6.25. To see this figure in color, go online.

The cholesterol-dependent cytolysin and cholesterol oxidase assays also report on the accessibility of membrane cholesterol but require a separate experiment for every χ_C tested. In addition, the experimental observable in our assay, namely membrane area visualized by fluorescence microscopy, enables us to directly witness any evidence of large-scale structural changes of the membrane during the course of our experiment. A disadvantage of our assay is that the signal/noise diminishes in the low-cholesterol regime ($\leq$30 mol %) because at these χ_C values, a_{avg} increases sharply as cholesterol is removed, meaning that large changes in χ_C yield very small changes in the total bilayer area remaining. Our discussion focuses on the accessibility of cholesterol. A vast literature of complementary techniques exists to assess cholesterol-lipid interactions and has been reviewed by others (72). As only one example, isothermal titration calorimetry detects nonideal lipid-cholesterol mixing in bilayers at $\chi_C \geq 0.3$, although the membrane partition coefficient of cholesterol appears to increase with χ_C (35).

CONCLUSIONS

We found that there are two populations of cholesterol with distinct accessibilities in lipid bilayers composed of DMPC, SOPC, or DOPC at high concentrations of cholesterol. The accessibility of cholesterol decreases sharply as the more accessible population is depleted from the bilayer, yielding a single abrupt change in slope in all three traces of k_D versus χ_C in Fig. 6. The proportion of cholesterol initially in the more accessible population increases with the degree of unsaturation of the PC-lipid tail. Treating the depletion rate coefficient as a measure of accessibility that is proportional to chemical activity (9), our results are consistent with cholesterol activity being higher in membranes comprised of monounsaturated lipids as compared to those comprised of saturated lipids. Our results are consistent with the condensed-complex and cholesterol bilayer domain models of lipid membranes and complement previous experiments using different systems to build a body of work elucidating how the chemical potential of cholesterol changes with its mole fraction in membranes (10–18). We converted our results into predictions about these two models (Table 6). Our assay enables robust determination of the accessibility of cholesterol in lipid bilayers as a function of both phospholipid structure and cholesterol concentration.

SUPPORTING MATERIAL

Supporting Materials and Methods, four figures, and five tables are available at http://www.biophysj.org/biophysj/supplemental/S0006-3495(15)01178-9.

AUTHOR CONTRIBUTIONS

J.P.L., T.P., and S.L.K. designed the research; J.P.L. performed the research; J.P.L. and N.T. analyzed the data; and J.P.L. and S.L.K. wrote the article.

ACKNOWLEDGMENTS

The authors thank Matthew C. Blosser for comments on the article.

This research was funded by the National Science Foundation (grant Nos. MCB-07444852 and MCB-1402059). J.P.L. and N.T. were supported by National Science Foundation Graduate Research Fellowships Nos. DGE-0718124 and DGE-1256082, respectively. T.P. was supported by the Raymond and Beverly Sackler Foundation and the Fondation Bettencourt Schueller.

REFERENCES

1. Steck, T. L., and Y. Lange. 2010. Cell cholesterol homeostasis: mediation by active cholesterol. *Trends Cell Biol.* 20:680–687.
2. Das, A., J. L. Goldstein, …, A. Radhakrishnan. 2013. Use of mutant 125I-perfringolysin O to probe transport and organization of cholesterol in membranes of animal cells. *Proc. Natl. Acad. Sci. USA.* 110:10580–10585.
3. Das, A., M. S. Brown, …, A. Radhakrishnan. 2014. Three pools of plasma membrane cholesterol and their relation to cholesterol homeostasis. *eLife.* 3:e02882.
4. Lange, Y., and T. L. Steck. 1996. The role of intracellular cholesterol transport in cholesterol homeostasis. *Trends Cell Biol.* 6:205–208.
5. Lange, Y., J. Ye, and T. L. Steck. 2004. How cholesterol homeostasis is regulated by plasma membrane cholesterol in excess of phospholipids. *Proc. Natl. Acad. Sci. USA.* 101:11664–11667.
6. Lange, Y., J. Ye, and T. L. Steck. 2014. Essentially all excess fibroblast cholesterol moves from plasma membranes to intracellular compartments. *PLoS One.* 9:e98482.
7. Kris-Etherton, P. M., and S. Yu. 1997. Individual fatty acid effects on plasma lipids and lipoproteins: human studies. *Am. J. Clin. Nutr.* 65 (*Suppl*):1628S–1644S.
8. Silvius, J. R. 2003. Role of cholesterol in lipid raft formation: lessons from lipid model systems. *Biochim. Biophys. Acta.* 1610:174–183.
9. Radhakrishnan, A., and H. M. McConnell. 2000. Chemical activity of cholesterol in membranes. *Biochemistry.* 39:8119–8124.
10. Nelson, L. D., A. E. Johnson, and E. London. 2008. How interaction of perfringolysin O with membranes is controlled by sterol structure, lipid structure, and physiological low pH: insights into the origin of perfringolysin O-lipid raft interaction. *J. Biol. Chem.* 283:4632–4642.
11. Flanagan, J. J., R. K. Tweten, …, A. P. Heuck. 2009. Cholesterol exposure at the membrane surface is necessary and sufficient to trigger perfringolysin O binding. *Biochemistry.* 48:3977–3987.
12. Sokolov, A., and A. Radhakrishnan. 2010. Accessibility of cholesterol in endoplasmic reticulum membranes and activation of SREBP-2 switch abruptly at a common cholesterol threshold. *J. Biol. Chem.* 285:29480–29490.
13. Moe, P. C., and A. P. Heuck. 2010. Phospholipid hydrolysis caused by *Clostridium perfringens* α-toxin facilitates the targeting of perfringolysin O to membrane bilayers. *Biochemistry.* 49:9498–9507.
14. Olsen, B. N., A. A. Bielska, …, D. S. Ory. 2013. The structural basis of cholesterol accessibility in membranes. *Biophys. J.* 105:1838–1847.
15. Gay, A., D. Rye, and A. Radhakrishnan. 2015. Switch-like responses of two cholesterol sensors do not require protein oligomerization in membranes. *Biophys. J.* 108:1459–1469.
16. Lange, Y., S. M. A. Tabei, …, T. L. Steck. 2013. Stability and stoichiometry of bilayer phospholipid-cholesterol complexes: relationship to cellular sterol distribution and homeostasis. *Biochemistry.* 52:6950–6959.
17. Wang, M. M., M. Olsher, …, P. L. G. Chong. 2004. Cholesterol superlattice modulates the activity of cholesterol oxidase in lipid membranes. *Biochemistry.* 43:2159–2166.
18. Ali, M. R., K. H. Cheng, and J. Huang. 2007. Assess the nature of cholesterol-lipid interactions through the chemical potential of

cholesterol in phosphatidylcholine bilayers. *Proc. Natl. Acad. Sci. USA.* 104:5372–5377.

19. Johnson, B. B., P. C. Moe, …, A. P. Heuck. 2012. Modifications in perfringolysin O domain 4 alter the cholesterol concentration threshold required for binding. *Biochemistry.* 51:3373–3382.
20. Beattie, M. E., S. L. Veatch, …, S. L. Keller. 2005. Sterol structure determines miscibility versus melting transitions in lipid vesicles. *Biophys. J.* 89:1760–1768.
21. Stevens, M. M., A. R. Honerkamp-Smith, and S. L. Keller. 2010. Solubility limits of cholesterol, lanosterol, ergosterol, stigmasterol, and β-sitosterol in electroformed lipid vesicles. *Soft Matter.* 6:5882–5890.
22. Yancey, P. G., W. V. Rodrigueza, …, G. H. Rothblat. 1996. Cellular cholesterol efflux mediated by cyclodextrins. Demonstration Of kinetic pools and mechanism of efflux. *J. Biol. Chem.* 271:16026–16034.
23. Melzak, K. A., S. A. Melzak, …, J. L. Toca-Herrera. 2012. Cholesterol organization in phosphatidylcholine liposomes: a surface plasmon resonance study. *Materials (Basel).* 5:2306–2325.
24. Mohwald, H. 1995. *In* Structure and Dynamics of Membranes, R. Lipowsky and E. Sackmann, editors. Elsevier, Amsterdam, the Netherlands, pp. 161–211.
25. Kučerka, N., J. F. Nagle, …, J. Katsaras. 2008. Lipid bilayer structure determined by the simultaneous analysis of neutron and x-ray scattering data. *Biophys. J.* 95:2356–2367.
26. Stottrup, B. L., D. S. Stevens, and S. L. Keller. 2005. Miscibility of ternary mixtures of phospholipids and cholesterol in monolayers, and application to bilayer systems. *Biophys. J.* 88:269–276.
27. Veatch, S. L., and S. L. Keller. 2003. Separation of liquid phases in giant vesicles of ternary mixtures of phospholipids and cholesterol. *Biophys. J.* 85:3074–3083.
28. Kilsdonk, E. P. C., P. G. Yancey, …, G. H. Rothblat. 1995. Cellular cholesterol efflux mediated by cyclodextrins. *J. Biol. Chem.* 270: 17250–17256.
29. Haynes, M. P., M. C. Phillips, and G. H. Rothblat. 2000. Efflux of cholesterol from different cellular pools. *Biochemistry.* 39:4508–4517.
30. Beseničar, M. P., A. Bavdek, …, G. Anderluh. 2008. Kinetics of cholesterol extraction from lipid membranes by methyl-β-cyclodextrin—a surface plasmon resonance approach. *Biochim. Biophys. Acta.* 1778: 175–184.
31. Huang, J., J. T. Buboltz, and G. W. Feigenson. 1999. Maximum solubility of cholesterol in phosphatidylcholine and phosphatidylethanolamine bilayers. *Biochim. Biophys. Acta.* 1417:89–100.
32. Silvius, J. R. 1982. *In* Lipid-Protein Interactions, P. C. Jost and O. H. Griffith, editors. Wiley, New York, pp. 239–281.
33. Marsh, D. 2010. Liquid-ordered phases induced by cholesterol: a compendium of binary phase diagrams. *Biochim. Biophys. Acta.* 1798: 688–699.
34. Hamai, C., P. S. Cremer, and S. M. Musser. 2007. Single giant vesicle rupture events reveal multiple mechanisms of glass-supported bilayer formation. *Biophys. J.* 92:1988–1999.
35. Tsamaloukas, A., H. Szadkowska, …, H. Heerklotz. 2005. Interactions of cholesterol with lipid membranes and cyclodextrin characterized by calorimetry. *Biophys. J.* 89:1109–1119.
36. Niu, S.-L., and B. J. Litman. 2002. Determination of membrane cholesterol partition coefficient using a lipid vesicle-cyclodextrin binary system: effect of phospholipid acyl chain unsaturation and headgroup composition. *Biophys. J.* 83:3408–3415.
37. Anderson, T. G., A. Tan, …, J. Seelig. 2004. Calorimetric measurement of phospholipid interaction with methyl-β-cyclodextrin. *Biochemistry.* 43:2251–2261.
38. Huang, Z., and E. London. 2013. Effect of cyclodextrin and membrane lipid structure upon cyclodextrin-lipid interaction. *Langmuir.* 29: 14631–14638.
39. Steck, T. L., J. Ye, and Y. Lange. 2002. Probing red cell membrane cholesterol movement with cyclodextrin. *Biophys. J.* 83:2118–2125.
40. Hamilton, J. A. 2003. Fast flip-flop of cholesterol and fatty acids in membranes: implications for membrane transport proteins. *Curr. Opin. Lipidol.* 14:263–271.
41. Bruckner, R. J., S. S. Mansy, …, J. W. Szostak. 2009. Flip-flop-induced relaxation of bending energy: implications for membrane remodeling. *Biophys. J.* 97:3113–3122.
42. Jo, S., H. Rui, …, W. Im. 2010. Cholesterol flip-flop: insights from free energy simulation studies. *J. Phys. Chem. B.* 114:13342–13348.
43. Schindelin, J., I. Arganda-Carreras, …, A. Cardona. 2012. Fiji: an open-source platform for biological-image analysis. *Nat. Methods.* 9:676–682.
44. Patil, A., D. Huard, and C. J. Fonnesbeck. 2010. PyMC: Bayesian stochastic modelling in Python. *J. Stat. Softw.* 35:1–81.
45. Hung, W.-C., M.-T. Lee, …, H. W. Huang. 2007. The condensing effect of cholesterol in lipid bilayers. *Biophys. J.* 92:3960–3967.
46. Pan, J., S. Tristram-Nagle, and J. F. Nagle. 2009. Effect of cholesterol on structural and mechanical properties of membranes depends on lipid chain saturation. *Phys. Rev. E Stat. Nonlin. Soft Matter Phys.* 80:021931.
47. Heftberger, P., B. Kollmitzer, …, G. Pabst. 2014. Global small-angle x-ray scattering data analysis for multilamellar vesicles: the evolution of the scattering density profile model. *J. Appl. Cryst.* 47:173–180.
48. Gallová, J., D. Uhríková, …, P. Balgavý. 2010. Partial area of cholesterol in monounsaturated diacylphosphatidylcholine bilayers. *Chem. Phys. Lipids.* 163:765–770.
49. Kučerka, N., J. Pencer, …, J. Katsaras. 2007. Influence of cholesterol on the bilayer properties of monounsaturated phosphatidylcholine unilamellar vesicles. *Eur. Phys. J. E Soft Matter.* 23:247–254.
50. Kučerka, N., J. Gallová, …, J. Katsaras. 2009. Areas of monounsaturated diacylphosphatidylcholines. *Biophys. J.* 97:1926–1932.
51. Kučerka, N., M.-P. Nieh, and J. Katsaras. 2011. Fluid phase lipid areas and bilayer thicknesses of commonly used phosphatidylcholines as a function of temperature 1808:2761–2771.
52. Koenig, B. W., and K. Gawrisch. 2005. Specific volume of unsaturated phosphatidylcholines in the liquid crystalline phase. *Biochim. Biophys. Acta.* 1715:65–70.
53. Greenwood, A. I., S. Tristram-Nagle, and J. F. Nagle. 2006. Partial molecular volumes of lipids and cholesterol. *Chem. Phys. Lipids.* 143:1–10.
54. Tristram-Nagle, S., Y. Liu, …, J. F. Nagle. 2002. Structure of gel phase DMPC determined by x-ray diffraction. *Biophys. J.* 83:3324–3335.
55. Uhríková, D., P. Rybár, …, P. Balgavý. 2007. Component volumes of unsaturated phosphatidylcholines in fluid bilayers: a densitometric study. *Chem. Phys. Lipids.* 145:97–105.
56. Huang, J., and G. W. Feigenson. 1999. A microscopic interaction model of maximum solubility of cholesterol in lipid bilayers. *Biophys. J.* 76:2142–2157.
57. Brzustowicz, M. R., V. Cherezov, …, S. R. Wassall. 2002. Controlling membrane cholesterol content. A role for polyunsaturated (docosahexaenoate) phospholipids. *Biochemistry.* 41:12509–12519.
58. Brzustowicz, M. R., V. Cherezov, …, S. R. Wassall. 2002. Molecular organization of cholesterol in polyunsaturated membranes: microdomain formation. *Biophys. J.* 82:285–298.
59. Baykal-Caglar, E., E. Hassan-Zadeh, …, J. Huang. 2012. Preparation of giant unilamellar vesicles from damp lipid film for better lipid compositional uniformity. *Biochim. Biophys. Acta.* 1818:2598–2604.
60. Chong, P. L.-G. 1994. Evidence for regular distribution of sterols in liquid crystalline phosphatidylcholine bilayers. *Proc. Natl. Acad. Sci. USA.* 91:10069–10073.
61. McConnell, H. M., and A. Radhakrishnan. 2003. Condensed complexes of cholesterol and phospholipids. *Biochim. Biophys. Acta.* 1610:159–173.
62. Preston Mason, R., T. N. Tulenko, and R. F. Jacob. 2003. Direct evidence for cholesterol crystalline domains in biological membranes: role in human pathobiology. *Biochim. Biophys. Acta.* 1610:198–207.

63. Ziblat, R., K. Kjaer, …, L. Addadi. 2009. Structure of cholesterol/lipid ordered domains in monolayers and single hydrated bilayers. *Angew. Chem. Int. Ed.* 48:8958–8961.

64. Raguz, M., L. Mainali, …, W. K. Subczynski. 2011. The immiscible cholesterol bilayer domain exists as an integral part of phospholipid bilayer membranes. *Biochim. Biophys. Acta.* 1808:1072–1080.

65. Varsano, N., I. Fargion, …, L. Addadi. 2015. Formation of 3D cholesterol crystals from 2D nucleation sites in lipid bilayer membranes: implications for atherosclerosis. *J. Am. Chem. Soc.* 137:1601–1607.

66. Ziblat, R., L. Leiserowitz, and L. Addadi. 2010. Crystalline domain structure and cholesterol crystal nucleation in single hydrated DPPC:Cholesterol:POPC bilayers. *J. Am. Chem. Soc.* 132:9920–9927.

67. Raguz, M., L. Mainali, …, W. K. Subczynski. 2011. Using spin-label electron paramagnetic resonance (EPR) to discriminate and characterize the cholesterol bilayer domain. *Chem. Phys. Lipids.* 164: 819–829.

68. Barrett, M. A., S. Zheng, …, M. C. Rheinstädter. 2013. Solubility of cholesterol in lipid membranes and the formation of immiscible cholesterol plaques at high cholesterol concentrations. *Soft Matter.* 9:9342–9351.

69. Mainali, L., M. Raguz, and W. K. Subczynski. 2013. Formation of cholesterol bilayer domains precedes formation of cholesterol crystals in cholesterol/dimyristoylphosphatidylcholine membranes: EPR and DSC studies. *J. Phys. Chem. B.* 117:8994–9003.

70. Toppozini, L., S. Meinhardt, …, M. C. Rheinstädter. 2014. Structure of cholesterol in lipid rafts. *Phys. Rev. Lett.* 113:228101.

71. Sugár, I. P., and P. L.-G. Chong. 2012. A statistical mechanical model of cholesterol/phospholipid mixtures: linking condensed complexes, superlattices, and the phase diagram. *J. Am. Chem. Soc.* 134:1164–1171.

72. Ohvo-Rekilä, H., B. Ramstedt, …, J. P. Slotte. 2002. Cholesterol interactions with phospholipids in membranes. *Prog. Lipid Res.* 41:66–97.

Supporting information for: Depletion with cyclodextrin reveals two populations of cholesterol in model lipid membranes

J. P. Litz,[†] N. Thakkar,[†,‡] T. Portet,[†] and S. L. Keller[*,†,¶]

†*Department of Chemistry, University of Washington, Seattle, Washington 98195-1700, United States*

‡*Department of Applied Mathematics, University of Washington*

¶*Department of Physics, University of Washington*

E-mail: slkeller@chem.washington.edu

Bilayer area per molecule

All data used to determine the average area per molecule in a bilayer as a function of the mole fraction of cholesterol, $a_{\text{avg}}(\chi_C)$, are given in Tables S1-S5. d_{pp} is the electron density peak-to-peak distance as determined by X-ray diffraction. d_{H1} is the distance from the peak of the electron density profile to the interface of the hydrocarbon region of the bilayer as determined by the joint analysis of X-ray and neutron scattering data. A_{UC} is the area per unit cell as determined by neutron scattering or the joint analysis of X-ray and neutron scattering data. V_L, V_H, and V_C are the volumes of a PC-lipid, a PC-headgroup, and cholesterol in a bilayer, respectively.

Data and uncertainties from references S1, S2, and S3 were interpreted from graphs. Uncertainties in S4, S5, and S6 were reported as less than 2%; we treated the uncertainty as ±2%.

Table S1: Literature d_{pp} and A_{UC}, and calculated a_{avg} values for DMPC.

χ_C	Lit. d_{pp} (Å)	Lit. A_{UC} (Å^2)	Ref.	Calc. a_{avg} (Å^2)
0.00	34.9 ± 0.7	59.8 ± 1.2	S5	59.8 ± 1.2
0.00	35.3 ± 0.3		S2	59.4 ± 1.9
0.00	35.9 ± 0.1		S1	58.1 ± 1.3
0.09	38.4 ± 0.1		S1	51.8 ± 1.9
0.10	38.3 ± 0.5		S2	51.8 ± 2.6
0.17	40.3 ± 0.1		S1	47.6 ± 1.6
0.20	41.5 ± 0.4		S2	45.4 ± 1.8
0.23	41.6 ± 0.1		S1	44.9 ± 1.4
0.29	42.5 ± 0.1		S1	43.2 ± 1.4
0.30	41.8 ± 0.5		S2	44.0 ± 1.9
0.36	43.2 ± 0.1		S1	41.8 ± 1.3
0.38	43.3 ± 0.1		S1	41.6 ± 1.3
0.41	43.3 ± 0.1		S1	41.4 ± 1.2
0.44	43.3 ± 0.1		S1	41.2 ± 1.2

Table S2: Literature d_{pp} and A_{UC}, and calculated a_{avg} values for SOPC.

χ_C	Lit. d_{pp} (Å)	Lit. A_{UC} (Å^2)	Ref.	Calc. a_{avg} (Å^2)
0.00	38.7 ± 0.8		S6	65.6 ± 3.7
0.00	38.6 ± 0.8	65.5 ± 1.3	S5	65.5 ± 1.3
0.00	39.0 ± 0.1		S1	65.0 ± 1.3
0.00	39.2 ± 0.3		S2	64.6 ± 1.8
0.09	40.8 ± 0.1		S1	59.4 ± 1.9
0.10	40.3 ± 0.5		S2	60.1 ± 2.7
0.14	41.7 ± 0.1		S1	56.7 ± 1.7
0.20	42.1 ± 0.5		S2	54.7 ± 2.3
0.20	42.1 ± 0.8		S6	54.7 ± 3.1
0.20	42.7 ± 0.1		S1	53.7 ± 1.6
0.28	43.8 ± 0.1		S1	50.4 ± 1.5
0.30	43.6 ± 0.3		S2	50.3 ± 1.7
0.38	44.8 ± 0.1		S1	47.1 ± 1.3
0.40	43.9 ± 0.5		S2	47.9 ± 1.9
0.44	44.6 ± 0.1		S1	46.2 ± 1.3
0.46	44.6 ± 0.1		S1	45.8 ± 1.3
0.47	44.6 ± 0.1		S1	45.6 ± 1.3
0.50	44.2 ± 0.5		S2	45.5 ± 1.8

Table S3: Literature d_{pp} and A_{UC}, and calculated a_{avg} values for DOPC.

χ_C	Lit. d_{pp} (Å)	Lit. A_{UC} (Å^2)	Ref.	Calc. a_{avg} (Å^2)
0.00		68.5 ± 2.3	S3	68.5 ± 2.3
0.00	36.6 ± 0.1		S1	67.9 ± 1.4
0.00	36.7 ± 0.3		S2	67.6 ± 1.9
0.00	36.9 ± 0.7		S6	67.2 ± 3.5
0.00	36.8 ± 0.7	67.4 ± 1.3	S4	67.4 ± 1.3
0.00		65.9 ± 1.3	S7	65.9 ± 1.3
0.09	38.0 ± 0.1		S1	62.7 ± 1.9
0.10	37.2 ± 0.5		S2	64.1 ± 2.9
0.14	38.7 ± 0.1		S1	60.1 ± 1.8
0.17		71.5 ± 2.4	S3	59.3 ± 2.0
0.17		70.8 ± 1.4	S7	58.8 ± 1.2
0.20	39.0 ± 0.5		S2	58.2 ± 2.5
0.20	40.9 ± 0.8		S6	54.9 ± 3.0
0.25	40.2 ± 0.1		S1	55.0 ± 1.5
0.29		76.2 ± 1.8	S7	54.1 ± 1.3
0.29		76.0 ± 2.9	S3	53.9 ± 2.0
0.30	39.9 ± 0.3		S2	54.4 ± 1.8
0.33	41.2 ± 0.1		S1	51.7 ± 1.4
0.34		79.3 ± 4.2	S3	53.1 ± 2.8
0.38		81.1 ± 3.0	S3	50.3 ± 1.9
0.38	41.6 ± 0.1		S1	50.1 ± 1.3
0.38		79.2 ± 2.4[a]	S7	49.1 ± 1.5
0.39	41.6 ± 0.1		S1	49.9 ± 1.3
0.40	40.4 ± 0.5		S2	51.5 ± 2.1
0.40	41.6 ± 0.1		S1	49.7 ± 1.3
0.44		86.2 ± 1.9	S3	48.3 ± 1.1
0.45		83.9 ± 2.7[a]	S7	46.1 ± 1.5
0.50		91.9 ± 4.1	S3	46.0 ± 2.1

[a]The authors reported signatures of pauci-lamellar vesicles in this sample.

Table S4: Literature d_{H1} values.

Lipid	d_{H1} (Å)	Ref.
DMPC	4.61 ± 0.09^a	S5
SOPC	4.35 ± 0.09^a	S5
DOPC	3.9 ± 0.1^a	S4

[a]There are no published values for the χ_C dependence of d_{H1} for these phospholipids, so we estimated uncertainties at $\pm 5\%$ for all $\chi_C > 0$.

Table S5: Literature V_L, V_H, and V_C values.

Lipid	V_L (Å^3)	V_H (Å^3)	V_C (Å^3)
DMPC ($\chi_C < 0.24$)	1099.6 ± 0.5^a	325 ± 6^c	565.1 ± 3.4^a
DMPC ($\chi_C \geq 0.24$)	1076.8 ± 1.3^a	325 ± 6^c	637.5 ± 1.8^a
SOPC	1309.5 ± 1.3^b	325 ± 6^c	630 ± 10^a
DOPC	1302.2 ± 0.4^a	325 ± 6^c	632.9 ± 0.9^a

[a]Reference S8. If not reported, the uncertainty was obtained by refitting published data. [b]Reference S9. [c]References S10 and S11. Uncertainty estimated from the spread of published values.

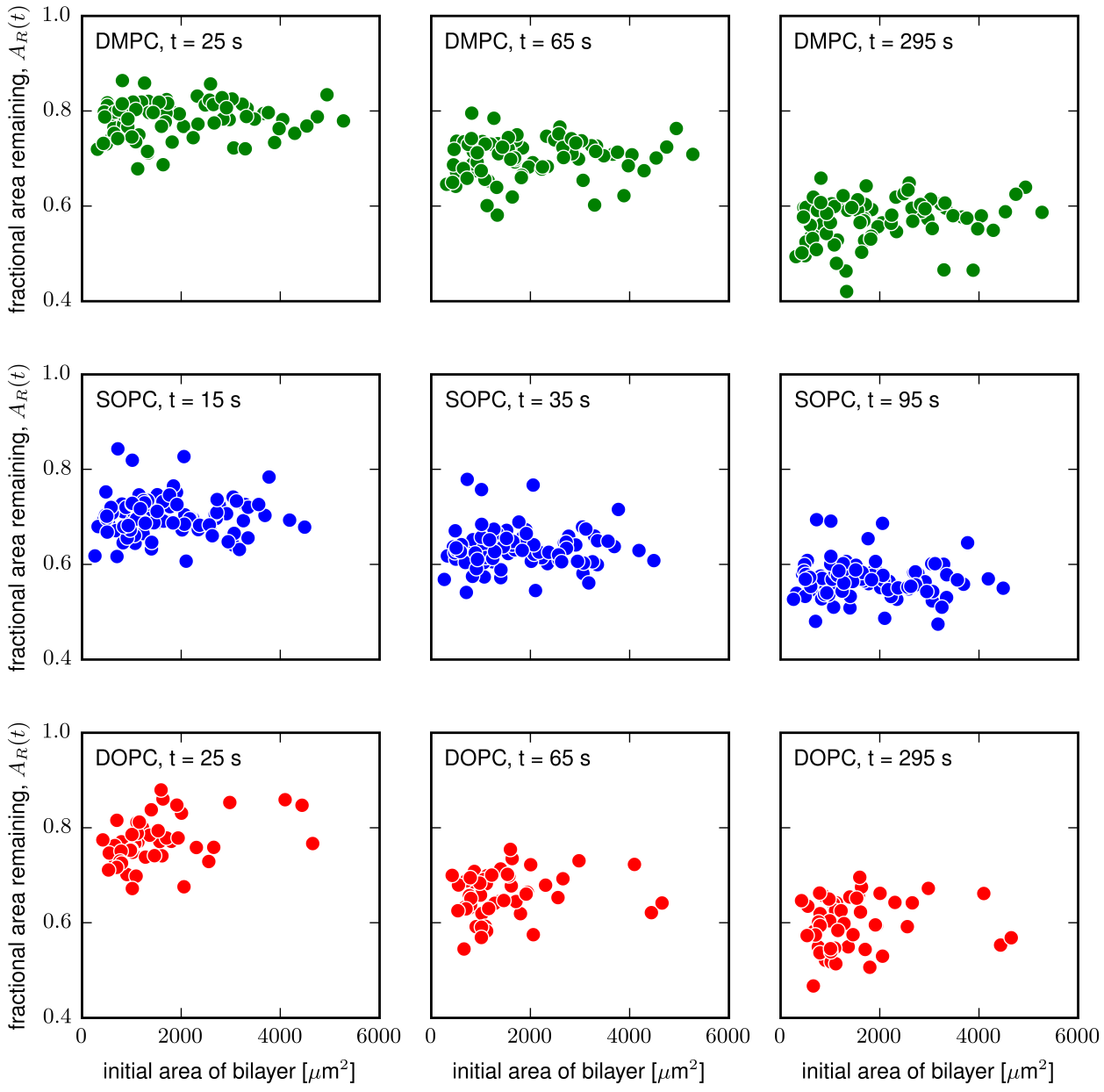

Figure S1: There is no apparent correlation between the initial area of the supported lipid bilayer and the fraction of bilayer area remaining as a function of time after mβCD is added, $A_R(t)$, for the systems we studied.

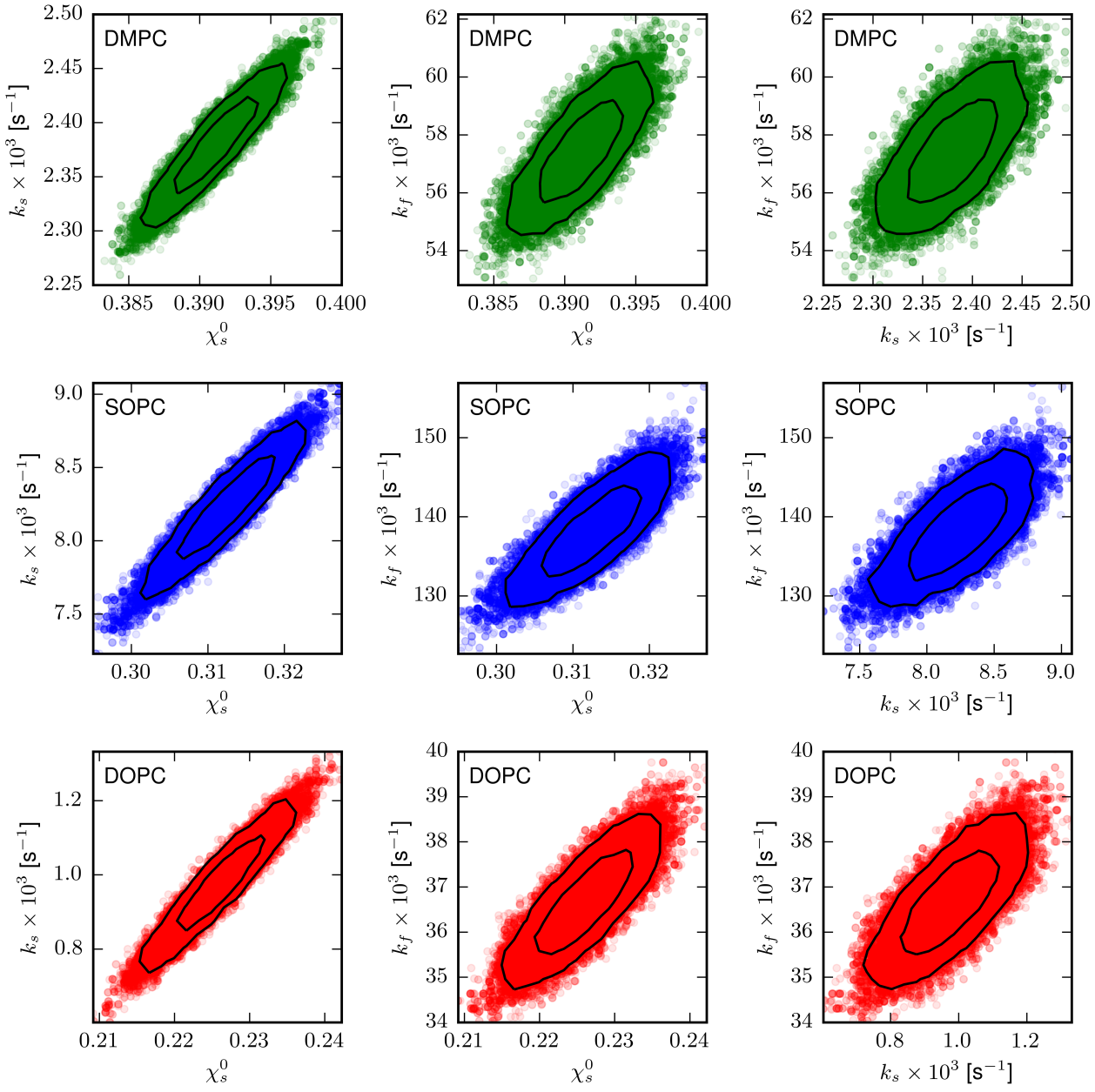

Figure S2: Samples from the posterior distribution of fitting parameters corresponding to the two cholesterol population model (see Fig 4, Table 2, and Eq. 10). Contours correspond to one and two standard deviations of the marginalized posterior samples.

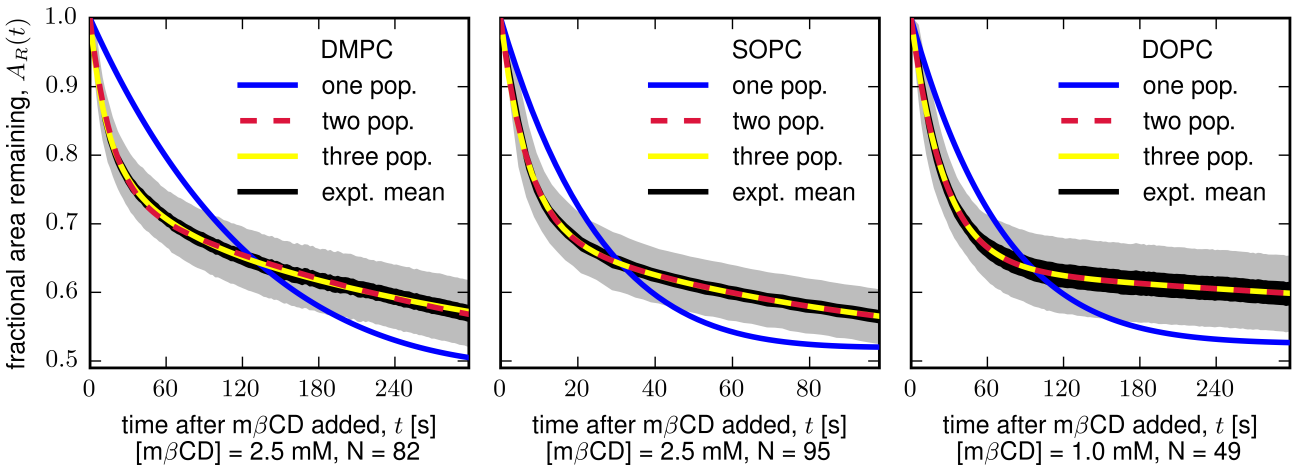

Figure S3: The fraction of bilayer area remaining as a function of time, $A_R(t)$ after addition of mβCD. The black region depicts our experimental mean ± two standard errors, and the gray region depicts the standard deviation of our data. The model with two cholesterol populations (three fitting parameters) describes our data well (crimson dotted line, main text eq. 10). The model with one cholesterol population (one fitting parameter, main text eq. 6) underfits our data (blue line). The model with three cholesterol populations (five fitting parameters, SI eq. 1) is unwarranted by our data (yellow line).

The equation of fit for the three population fit is

$$A_R(t) = \left(1 - \chi_C(0) + \chi_1 e^{-k_1 t} + \chi_2 e^{-k_2 t} + (\chi_C(0) - \chi_1 - \chi_2) e^{-k_3 t}\right) \times \frac{a_{\text{avg}}(\chi_C[t])}{a_{\text{avg}}(\chi_C[0])}, \qquad (1)$$

where χ_1, χ_2, k_1, k_2, and k_3 are the five fitting parameters.

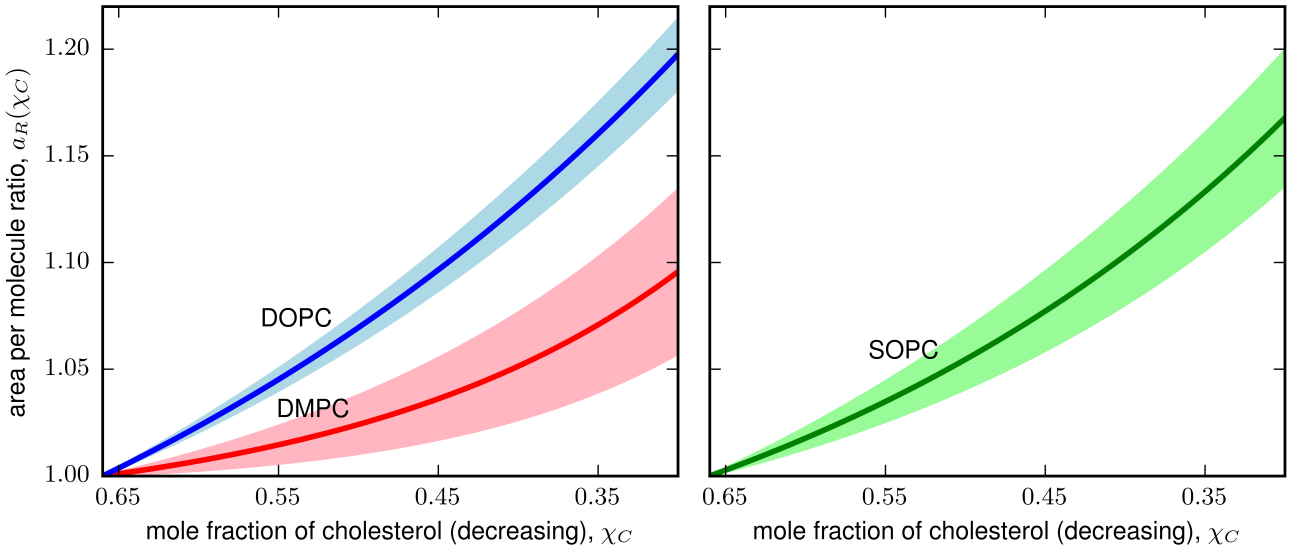

Figure S4: The average area per molecule ratio as a function of the mole fraction of cholesterol, $a_R(\chi_C)$ (solid lines) and the uncertainty in these values (one standard deviation, encompassed by the shaded area overlaying each line). Eq. 1 of the main text shows how the observable of our experiments, the fraction of bilayer area remaining as a function of time $A_R(t)$, is proportional to the ratio of the average area per molecule in the bilayer at time t and the average area per molecule in the bilayer at time $t = 0$. This figure shows that over the regime of $\chi_C > 0.3$ in which our experiment takes place, uncertainty resulting from $a_R(\chi_C)$ is small.

We define the average area per molecule ratio as follows:

$$a_R(\chi_C) = \frac{a_{\text{avg}}(\chi_C)}{a_{\text{avg}}(\chi_C = 0.66)}. \tag{2}$$

References

(S1) Hung, W.-C.; Lee, M.-T.; Chen, F.-Y.; Huang, H. W. *Biophys. J.* **2007**, *92*, 3960–3967.

(S2) Pan, J.; Tristram-Nagle, S.; Nagle, J. F. *Phys. Rev. E* **2009**, *80*, 021931.

(S3) Gallová, J.; Uhríková, D.; Kučerka, N.; Teixeira, J.; Balgavý, P. *Chem. Phys. Lipids* **2010**, *163*, 765–770.

(S4) Kučerka, N.; Gallova, J.; Uhríková, D.; Balgavý, P.; Bulacu, M.; Marrink, S.-J.; Katsaras, J. *Biophys. J.* **2009**, *97*, 1926–1932.

(S5) Kučerka, N.; Nieh, M.-P.; Katsaras, J. *BBA-Biomembranes* **2011**, *1808*, 2761–2771.

(S6) Heftberger, P.; Kollmitzer, B.; Heberle, F. A.; Pan, J.; Rappolt, M.; Amenitsch, H.; Kučerka, N.; Katsaras, J.; Pabst, G. *J. Appl. Crystallogr.* **2014**, *47*, 173–180.

(S7) Kučerka, N.; Pencer, J.; Nieh, M.-P.; Katsaras, J. *Eur. Phys. J. E* **2007**, *23*, 247–254.

(S8) Greenwood, A. I.; Tristram-Nagle, S.; Nagle, J. F. *Chem. Phys. Lipids* **2006**, *143*, 1–10.

(S9) Koenig, B. W.; Gawrisch, K. *BBA-Biomembranes* **2005**, *1715*, 65–70.

(S10) Tristram-Nagle, S.; Liu, Y.; Legleiter, J.; Nagle, J. F. *Biophys. J.* **2002**, *83*, 3324–3335.

(S11) Uhríková, D.; Rybár, P.; Hianik, T.; Balgavý, P. *Chem. Phys. Lipids* **2007**, *145*, 97–105.